


Stable Scalp EEG Spatospectral Patterns Across Paradigms Estimated by Group ICA

René Labounek^{1,2,3}  · David A. Bridwell⁴ · Radek Mareček² · Martin Lamoš^{1,2} · Michal Míkl² · Tomáš Slavíček^{1,2} · Petr Bednařík^{2,5,6} · Jaromír Baštinec⁷ · Petr Hlušík^{3,8} · Milan Brázdil² · Jiří Jan¹

Received: 4 October 2016 / Accepted: 18 August 2017 / Published online: 5 September 2017
© Springer Science+Business Media, LLC 2017

Abstract Electroencephalography (EEG) oscillations reflect the superposition of different cortical sources with potentially different frequencies. Various blind source separation (BSS) approaches have been developed and implemented in order to decompose these oscillations, and a subset of approaches have been developed for decomposition of multi-subject data. Group independent component analysis (Group ICA) is one such approach, revealing spatospectral maps at the group level with distinct frequency and spatial characteristics. The reproducibility of these distinct maps across subjects and paradigms is relatively unexplored domain, and the topic of the present study. To address this, we conducted separate group ICA decompositions of EEG spatospectral patterns on data collected during three different paradigms or tasks (resting-state, semantic decision task and visual oddball task). K-means clustering analysis of back-reconstructed individual subject maps demonstrates

that fourteen different independent spatospectral maps are present across the different paradigms/tasks, i.e. they are generally stable.

Keywords EEG · ICA · Spatospectral patterns · Multi-subject blind source separation · Resting-state · Semantic decision · Visual oddball

Introduction

Scalp electrical fluctuations (measured with electroencephalography; EEG) are related to a range of cognitive processes, and different processes are often associated with different frequencies (Buzsaki 2006). These potentially distinct processes sum together due to the volume conduction properties of the brain, skull, and scalp resulting in spatial smearing of voltages on the surface of the scalp (Nunez and Srinivasan 2006).

Blind source separation (BSS) approaches are useful for decomposing voltage mixtures measured from electrodes placed on the scalp surface, and temporal independent component analysis (ICA) is one of the most often used BSS algorithms. Temporal ICA decomposes the electrode × time

This is one of several papers published together in Brain Topography on the “Special Issue: Multisubject decomposition of EEG - methods and applications”.

Electronic supplementary material The online version of this article (doi:10.1007/s10548-017-0585-8) contains supplementary material, which is available to authorized users.

✉ René Labounek
rene.labounek@gmail.com

¹ Department of Biomedical Engineering, Brno University of Technology, Brno, Czech Republic

² Central European Institute of Technology, Masaryk University, Brno, Czech Republic

³ Department of Neurology, Palacký University, Olomouc, Czech Republic

⁴ Mind Research Network, Albuquerque, NM 87106, USA

⁵ Center for Magnetic Resonance Research, University of Minnesota, Minneapolis, MN, USA

⁶ Division of Endocrinology and Diabetes, University of Minnesota, Minneapolis, MN, USA

⁷ Department of Mathematics, Brno University of Technology, Brno, Czech Republic

⁸ Department of Neurology, University Hospital Olomouc, Olomouc, Czech Republic

matrix into a source \times time matrix with an associated mixing matrix (i.e. scalp topography) (Makeig et al. 1997; Hyvärinen et al. 2001; Stone 2004). Temporal ICA is widely implemented for removing eye blink and eye movement artifacts, but appears less successful in decomposing distinct EEG oscillations measured in the absence of an explicit task (i.e. during ‘rest’) (Hyvärinen et al. 2010; Li et al. 2015).

In order to isolate distinct EEG oscillations (i.e. signal from signal), a variety of approaches have been developed to decompose real valued or complex valued EEG spectra (Anemüller et al. 2003; Bernat et al. 2005; Onton et al. 2005; Hyvärinen et al. 2010; Nikulin et al. 2011; Ramkumar et al. 2012; Shou et al. 2012; Kauppi et al. 2013; Hu et al. 2015; Van Der Meij et al. 2016; Takeda et al. 2016). These approaches are generally applied to individual subjects data, which requires identification of similar components across the separate decompositions. In order to overcome this problem, and in order to aggregate information across the aggregate group for decomposition, various multi-subject extensions have been developed and implemented (Kovacevic and McIntosh 2007; Congedo et al. 2010; Eichele et al. 2011; Cong et al. 2013; Lio and Boulinguez 2013; Bridwell et al. 2013, 2014, 2015; Ponomarev et al. 2014; Ramkumar et al. 2014; Huster et al. 2015; Mareček et al. 2016).

Spatiospectral group ICA decompositions have been applied to EEG data collected at rest, revealing biologically plausible spatio-spectral maps (i.e. with interpretable frequency and spatial characteristics) (Wu et al. 2010; Bridwell

et al. 2016), and fluctuations in map time courses have been associated with BOLD signal fluctuations in concurrently recorded fMRI data (Bridwell et al. 2013; Yu et al. 2016).

However, the stability of spatio-spectral components across different experiments has yet to be explored. We focus on this question explicitly within the present manuscript by conducting k-means clustering analysis of spatio-spectral maps derived from three different EEG datasets [visual oddball task (VOT), semantic decision task (SDT) and resting-state paradigm (RST)], revealing the characteristics, properties, and similarity/dissimilarity of maps over datasets, and the relationship between spatio-spectral map time courses and the stimulus vector time courses. Overall, spatio-spectral maps are generally stable across different paradigms, which motivates the utility of the approach for further studies isolating distinct EEG spatio-spectral functional responses that contribute to cognitive function, and may differ between healthy and clinical populations.

Materials and Methods

Figure 1 illustrates the pipeline from the original EEG collected during the three paradigms, to assessment of component stability by k-means clustering of individual subject component maps. Each step within the block diagram is described in more detail below.

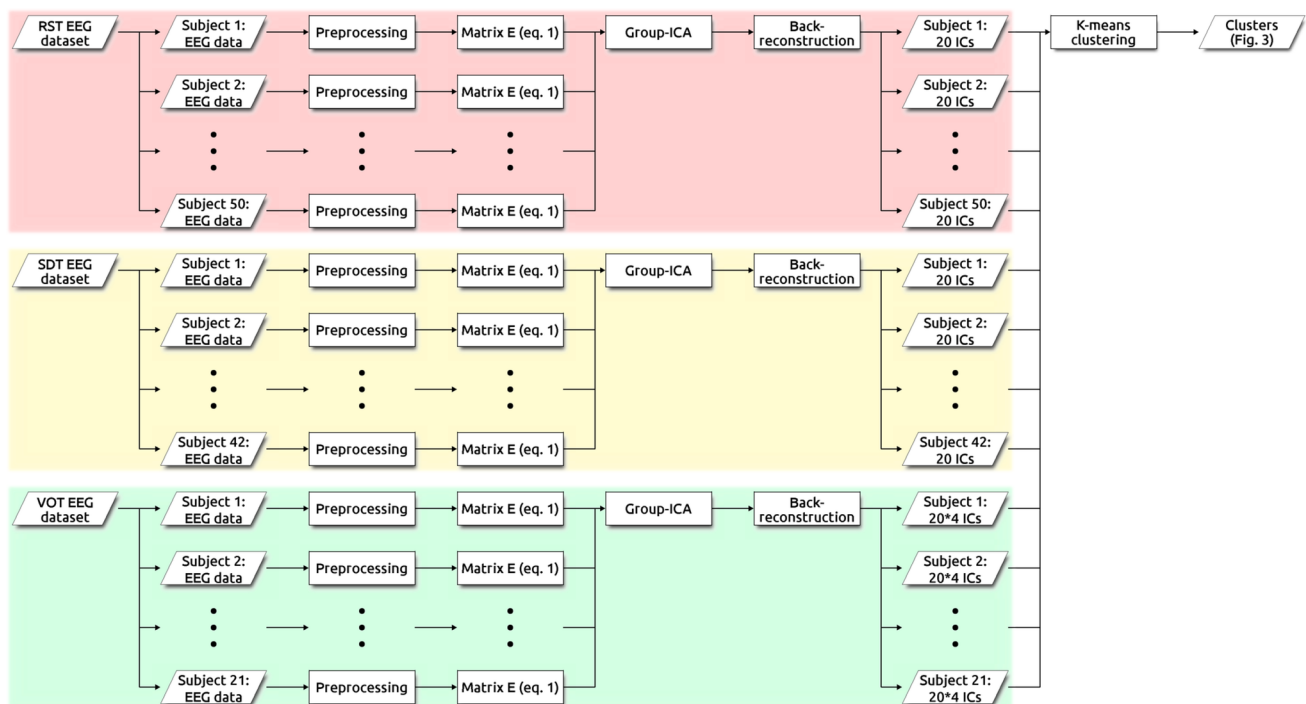


Fig. 1 Block diagram of the analysis pipeline from resting-state (RST), semantic decision (SDT) and visual oddball (VOT) EEG datasets

EEG Acquisition

The scalp EEG data, with a reference between Cz and Fz electrodes, was acquired simultaneously with fMRI using an MR compatible 32-channel 10/20 EEG system (*Brain-Products, Germany*) with a sampling frequency of 5 kHz. Two channels were used for ECG and EOG. The simultaneous fMRI data was acquired using 1.5T Siemens Symphony Numaris. However, the present manuscript focuses on the EEG data only. Informed consent was obtained from all subjects after the procedures were fully explained, and the study received the approval by the local ethics committee. The equipment was identical during acquisitions of the three paradigms described below, and the subjects within two paradigms partially overlapped (among the 50 and 42 individuals who participated in the resting state and semantic decision paradigms, respectively, 29 subjects participated in both). The VOT participants were a separate group of subjects than the other two tasks.

Resting-State Paradigm and fMRI Acquisition

Fifty healthy subjects participated in a 15 min “resting-state” experiment (30 right handed men, 20 right-handed women; age 25 ± 5 years). Subjects were instructed to lie still within the fMRI scanner with their eyes closed, not to think of anything specific, and not to fall asleep.

Gradient Echo, Echo-Planar Functional Imaging Sequence TR=3000 ms; TE=40 ms; FOV=220×220 mm; FA=90°; matrix size 64×64 (3.9×3.9 mm); slice thickness=3.5 mm; and 32 transversal slices which covered the whole brain excluding part of the cerebellum. 300 functional scans were acquired in 1 continuous session.

Semantic Decision Paradigm and fMRI Acquisition

A block designed semantic decision task was performed by 42 healthy subjects (22 right-handed men, 2 left-handed men, 18 right-handed women; age 25 ± 5 years). The task was designed with a block stimulation paradigm, with the goal of eliciting robust language network activation. During the probe block, two types of sentences were presented in random order. Sentences with semantic error created by a phonemic exchange (e.g. The cat was chased by fog) alternated with semantically correct sentences. The sentences were replaced with a series of the characters X or O, (e.g. ‘Xxxx xx xxxx xxx.’) during the control block. Nine control and eight probe blocks alternated during the experiment. Each block lasted 24 s, and consisted of six different control or probe stimuli presented for 3.5 s followed by a black screen for 0.5 s. Subjects viewed the stimuli through a mirror

mounted on the head coil. Responses were not requested from the subjects during the task. After the session, no subjects reported any problems with reading the sentences (Mareček et al. 2016).

Gradient Echo, Echo-Planar Functional Imaging Sequence TR=1850 ms, TE=40 ms, FOV=250×250 mm; FA=80°, matrix size=64×64 (3.9×3.9 mm); slice thickness=6 mm; no gap between slices; 20 transversal slices per scan which covered the whole brain excluding part of the cerebellum. 228 functional scans were acquired in 1 continuous session.

Visual Oddball Paradigm and fMRI Acquisition

An event-related designed visual oddball task was performed by 21 healthy subjects (13 right-handed men, 1 left-handed man, 7 right-handed women; age 23 ± 2 years). Three stimulus types were presented randomly to each subject. Each stimulus consisted of a single yellow uppercase letter shown for 500 ms on a black background. Inter-stimulus intervals were either 4, 5 or 6 s (drawn uniformly and randomly). A total of 336 stimuli were presented, consisting of targets (letter X, 15%), frequent (letter O, 70%) and distractors (letters other than X and O, 15%). Subjects were instructed to press a button held in their right hand whenever the target stimulus appeared and not to respond to distractor or frequent stimuli. The experiment was divided into 4 sessions for each person (84 stimuli per session) (Brázdil et al. 2007; Labounek et al. 2015).

Gradient Echo, Echo-Planar Functional Imaging Sequence TR=1660 ms; TE=45 ms; FOV=250×250 mm; FA=80°; matrix size=64×64 (3.9×3.9 mm); slice thickness=6 mm; 15 transversal slices per scan which covered the whole brain excluding part of the cerebellum. The whole task was divided into four equal runs of 256 scans and 84 stimuli.

EEG Data Preprocessing

We preprocessed the EEG data using BrainVision Analyzer 2.02 (*BrainProducts, Germany*). Gradient artifacts were removed using template subtraction (Allen et al. 2000) and signals were resampled to 250 Hz (antialiasing filter included), and filtered with a Butterworth zero phase 1 Hz–40 Hz band-pass filter. Cardiobalogram artifacts were removed by subtracting the average pulse artifact waveform from each channel (Allen et al. 1998) and signals were re-referenced to the average. For visual oddball EEG data, eye-blinking artifacts were removed by conducting a temporal ICA decomposition and removing eye-blink artifacts from the back-reconstructed time course.

Overview of Spatospectral Group ICA

Group ICA was implemented using the GIFT software package (Calhoun et al. 2001; <http://mialab.mrn.org/software/gift/>) with the INFOMAX ICA algorithm (Bell and Sejnowski 1995; Bridwell et al. 2016). Group ICA extends the single subject implementation of ICA to operate on multi-subject datasets, returning components estimated at the aggregate group level while preserving individual subject variability (Allen et al. 2012; for review see; Calhoun and Adalı 2012). Individual subject estimates are derived by back-reconstructing the group components on the individual subject data using either PCA based back-reconstruction (i.e. the individual partition of the PCA reducing matrix is matrix multiplied by the individual partition of the aggregate reducing matrix) (Calhoun et al. 2001), or spatio-temporal regression (STR) (i.e. dual regression, an indirect least squares approach) (Calhoun et al. 2004; for review see; Erhardt et al. 2011). The individual subject mixing matrices represent the contribution of the group component to each epoch, and the temporal modulation of each component is conceptually similar to the envelope of the response within the frequency band defined by that component.

Temporal and spectral decompositions of EEG are often implemented, with unique merits and limitations to each approach. The algorithmic assumptions of temporal ICA align well with the biological generation of EEG, where the voltage at each electrode reflects a linear mixture of independent scalp voltages (Makeig et al. 2004; Onton et al. 2006). However, while temporal ICA is well suited for removing artifacts (e.g. eye movement and eye blink), it appears less well suited at decomposing distinct EEG oscillations (i.e. EEG signal from EEG signal) compared to alternative approaches including (but not limited to) second-order blind identification (SOBI) (Belouchrani et al. 1997; Tang et al. 2005; Tang 2010), approximate joint diagonalization of cospectra (AJDC) (Congedo et al. 2008, 2010), or spectral ICA (Hyvärinen et al. 2010; Bridwell et al. 2016).

In the context of spatospectral ICA implemented here, we assume that the [frequency \times channel] amplitude data at each epoch reflects a linear mixture of independent [frequency \times channel] amplitude maps. The assumption of linear mixing of independent spatospectral maps is less theoretically tied to the biological generation of EEG (i.e. a linear mixture of temporal sources at each electrode), but appears to have utility nonetheless, analogous to the utility of applying spatial ICA to fMRI data despite the known interdependence and connectivity among brain networks. Importantly, Bridwell et al. (2016) demonstrate that spatospectral ICA may be successfully implemented to decompose biologically plausible simulations of spatospectral maps with source distributions and dependencies that are less than optimal for many BSS algorithms. These findings indicate that

INFOMAX ICA is robust to the source characteristics of realistic EEG spatospectral maps. Bridwell et al. (2016) also demonstrate that similar components may be derived using INFOMAX ICA and weights adjusted with second-order blind identification (WASOBI) (Belouchrani et al. 1997; Yeredor 2000; Doron and Yeredor 2004; Tichavský et al. 2006), two approaches with different algorithmic assumptions.

EEG Spatospectral Decomposition

For each session, the preprocessed EEG signal from each lead was normalized such that the time course was normally distributed $N(0,1)$, and divided into 1.66 s (the shortest repetition time of fMRI scanning TR) epochs without overlap. Each epoch was transformed to the spectral domain with fast Fourier transform (FFT), generating a vector (length = 67) of complex valued spectral coefficients between 0–40Hz. Complex values were converted to absolute power by taking the absolute value and squaring. The output vector of 67 real absolute power values comprised a 3D matrix E with dimensions n_t , n_c and n_ω . Dimension n_t is the total number of EEG epochs ($n_t = 540$ for RST; $n_t = 255$ for SDT; $n_t = 256$ for VOT), dimension n_c is the total number of leads ($n_c = 30$) and dimension n_ω is the total number of spectral coefficients ($n_\omega = 67$). The 3D matrix $E(n_t, n_c, n_\omega)$ was transformed into a 2D matrix $E(n_t, n_c * n_\omega)$ and used as input into group spatospectral ICA decomposition (Eq. 1) (Bridwell et al. 2013), returning a group mixing matrix W with dimensions $W(n_t, m)$ and a group source matrix S with dimensions $S(m, n_c * n_\omega)$. The dimension m is the number of decomposed orthogonal and independent components.

$$E = WS \quad (1)$$

Group spatospectral ICA was conducted separately for each paradigm and the data were decomposed to $m = 20$ orthogonal and independent spatospectral components, after reducing the dimensionality of each single-subject 2D matrix E with PCA (principal component analysis; reduced at 50 PCs). The PCA data reduction and whole group ICA decomposition were performed using the GIFT toolbox (Calhoun et al. 2001) with the INFOMAX algorithm (Bell and Sejnowski 1995; Bridwell et al. 2016). The reproducibility of group components was examined using the ICASSO package (Himberg and Hyvärinen 2003; Himberg et al. 2004), which conducts multiple group ICA runs on the same dataset (ten iterations). ICASSO employs the hierarchical clustering method to split up all components from all runs into a predefined number of clusters, and the reproducibility of each group component is estimated within a given Group ICA run by computing the cluster quality index I_q (Himberg et al. 2004). The cluster quality index reflects the compactness and uniqueness of a given cluster of components,

computed as the difference between the average intra-cluster similarity and the average inter-cluster similarity.

The analysis outputs are group-derived matrices \mathbf{W} and \mathbf{S} for each paradigm and separate \mathbf{W} and \mathbf{S} matrices generated by back reconstruction against each individual subject's data. The \mathbf{S} spatio-spectral matrices were collected across subjects and paradigms for clustering, as described below. The relationship between spatio-spectral components/sources and task dynamics were examined by relating the source time course (i.e. mixing matrix) \mathbf{W} with the respective stimulus time course.

Clustering of Spatio-spectral Maps Across Paradigms

For each subject, paradigm and session (4 sessions for VOT data), we have one matrix \mathbf{S} with dimensions $\mathbf{S}(20, 2010)$ containing 20 back-reconstructed spatio-spectral patterns. For similarity/dissimilarity assessment of the spatio-spectral patterns across paradigms, we have performed k-means clustering, a conventional algorithm belonging to multivariate methods for dimensionality reduction. Because we had 50 single-subject \mathbf{S} matrices for “rest”, 42 single-subject \mathbf{S} matrices for semantic decision task and $21 \times 4 = 84$ single-subject \mathbf{S} matrices for visual oddball task, there are $(50 + 42 + 84) \times 20 = 3520$ different spatio-spectral patterns comprising matrix \mathbf{C} , with dimensions $\mathbf{C}(3520, 2010)$ for input into k-means clustering. K-means clustering was performed with Pascual-Marqui et al. (1995) optimizing method with 40 final clusters. Clustering was repeated 50 times with random initial conditions and the result with minimal residuals was selected as the final clustering result.

After clustering, a few post-processing steps were necessary in some cases: IF a given cluster consists of spatio-spectral patterns from subjects from RST, subjects from SDT and subjects from VOT; AND IF another cluster contains the same spatio-spectral pattern with subjects from the three paradigms then those 2 clusters are combined and considered as one final cluster. This occurred in 3 of the 30 final clusters (cl. n. 2, 4 and 5). Clusters that were grouped together are indicated by { } brackets.

Intra-Cluster and Inter-Cluster Correlations

The correlation was computed between single-subject, single-session and single-paradigm spatio-spectral patterns within the k-means cluster (intra-cluster correlations) and between patterns of different clusters (inter-cluster correlations). These correlations were averaged separately within and across clusters to assess the similarity of patterns within clusters compared to across clusters. The mean coefficients (r) were transformed at t -values (Eq. 2), and then respectively at p -values (Eq. 3) of statistical significance characterizing the probability if intra- or inter-cluster components are similar or not (number of samples

$n=2010$). The function C in Eq. 3 is the cumulative density function for t -distribution depending on $|t|$ -value and on the difference between number of samples n and degrees of freedom ($=1$).

$$t = \frac{r}{\sqrt{\frac{1-r^2}{n-2}}} \quad (2)$$

$$p = 2(1 - C(|t|, n - 1)) \quad (3)$$

Comparison of EEG Spatio-spectral Pattern Dynamics with Stimuli Vectors

For each subject, paradigm and session, we have one matrix \mathbf{W} with dimensions $\mathbf{W}(n_t, 20)$ containing the back-reconstructed time course of each spatio-spectral component. Relationships between these dynamics and stimulus vector timings (in matrix \mathbf{X}) were assessed with a single-subject general linear model (Eq. 4, GLM) solved with the least mean square algorithm (Eq. 5) and a continuous group one-sample t -test for the k -th stimulus vector (Eq. 6) as implemented previously (Friston et al. 1994; Labounek et al. 2015). Variable \mathbf{c} is the vector of binary positive contrast at the stimulus vector of interest, the brackets $\langle \rangle$ characterize the expectation over subjects, variable σ is the standard deviation and variable s is the total number of subjects.

For VOT data, model matrix \mathbf{X} contained frequent, target and distractor timings in 12 separate binary vectors for each stimulus and session and 4 vectors for the DC component in each session. For SDT data, model matrix \mathbf{X} contained a binary vector with the probe block timings and a vector with the DC component.

$$\mathbf{W} = \mathbf{X}\boldsymbol{\beta} + \boldsymbol{\varepsilon} \quad (4)$$

$$\boldsymbol{\beta} = (\mathbf{X}^T\mathbf{X})^{-1}\mathbf{X}^T\mathbf{W} \quad (5)$$

$$t_k = \sqrt{s} \frac{\mathbf{c}_k^T \boldsymbol{\beta}_k}{\sigma_{\mathbf{c}_k^T \boldsymbol{\beta}_k}} \quad (6)$$

Results

EEG Spatio-spectral Patterns Over Datasets

The percent of variance explained after dimensionality reduction through PCA is demonstrated in Fig. 2a for the RST dataset, in Fig. 2b for the SDT dataset and in Fig. 2c for the VOT dataset. In all three cases, the first 50 principal components explain about 95% of variability.

The 20 independent group EEG spatio-spectral components, and their reproducibility over 10 ICASSO estimates are shown in Fig. S1 for RST data, Fig. S2 for SDT data

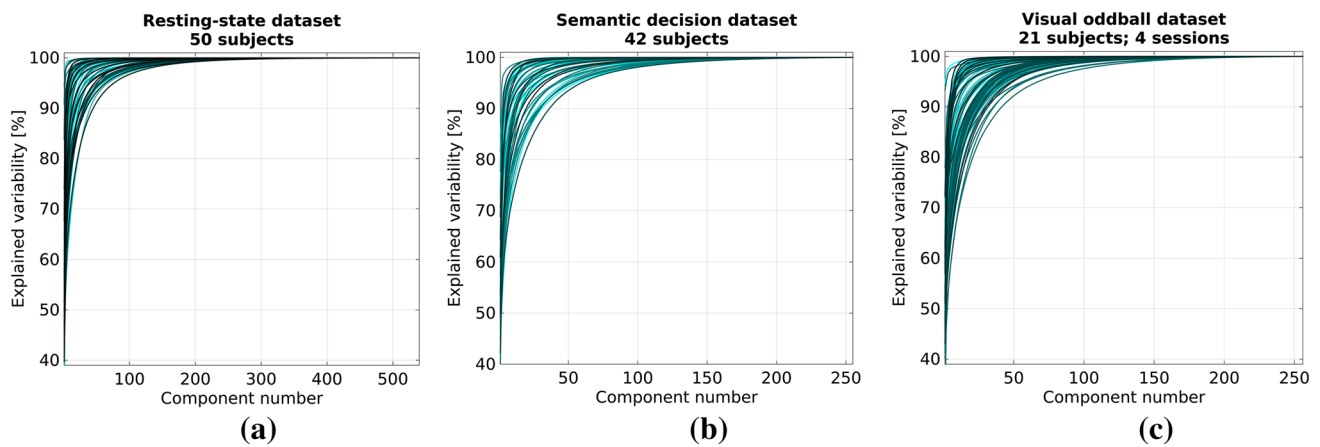


Fig. 2 EEG data dimensionality after PCA decomposition

and Fig. S3 for VOT data. The most reproducible component estimates were achieved for the resting-state paradigm (Fig. S1b, c) where all cluster quality values were above 0.9. The last 3 or 4 cluster quality indexes of the least reliable components were between 0.7 and 0.9 for semantic decision (Fig. S2b, c) and visual oddball (Fig. S3b, c) data. Visual inspection among the spatio-spectral maps generated across paradigms (Fig. S1a, Fig. S2a, and Fig. S3a) suggests that similar components may be observed across all three datasets (e.g. RST com. n. 10, SDT com. n. 14 and VOT com. n. 17; or RST com. n. 19, SDT com. n. 13 and VOT com. n. 13; or RST com. n. 16, SDT com. n. 15 and VOT com. n. 15; etc.), as evaluated empirically using k-means clustering of back-reconstructed individual results (next section).

K-Means Clustering

The original 3520 dimensions (i.e. 3520 spatio-spectral patterns) were reduced to 40 representative cluster centroids. Forty output clusters were selected after examining the compactness, i.e. σ_{mcv} (characterizing predictive residual variance with Eq. 22 derived in (Pascual-Marqui et al. 1995)) and σ_{μ} (characterizing residual variance with Eq. 10 derived in (Pascual-Marqui et al. 1995)) of clusters generated with 2–250 output centroids, and identifying the lowest norm at 40 (see Fig. S4). The relationships and distances among the 40 centroids are demonstrated within the dendrogram in Fig. 3a.

The cluster spatio-spectral features were examined by averaging the patterns separately for each experimental paradigm. These maps appear similar across the three paradigms in instances where many subjects contributed clusters to the average maps, as indicated by cluster 39 within Fig. 3b. The similarity of patterns within a representative cluster was demonstrated by computing the correlations between spatio-spectral patterns within cluster 39 (intra-cluster correlation)

and between cluster 39 and the patterns within each of the other clusters (inter-cluster correlations) (Fig. 4). The intra-cluster correlations were significantly larger than zero ($t=21.67$; $p=2.2*10^{-16}$), while the inter-cluster correlation values did not statistically differ from zero (|t| values ranged from 0.21 to 1.85 and p-values ranged from $6.5*10^{-2}$ to $8.35*10^{-1}$ respectively). Since the distributions within Fig. 4 appear symmetric around the mean, the mean intra-cluster and inter-cluster correlation coefficients are indicated within Fig. 5a as a summary of the the original 3520×3520 similarity matrix used for k-means clustering. The figure indicates that the majority of inter-cluster correlation coefficients did not statistically differ from 0, while all mean intra-cluster coefficients were significantly larger than 0 (Fig. 5b–d).

The percentage of subjects with maps present within each cluster is indicated within Table 1, separately for each paradigm, and a representative spatio-spectral map is indicated within Fig. 6 for each cluster. The radial projection of the post-processed dendrogram (containing 30 final clusters) and detailed visualization of each cluster for different paradigms are indicated within supplementary Fig. S5. The same dendrogram projection is shown also within Fig. 6.

K-means clustering analysis and Table 1 indicate that similar EEG spatio-spectral patterns appear across different tasks. Fifteen clusters (cl. numbers 2, 4, 5, 9, {13;3}, 16, {17;27}, {18;20}, 30, 32, 37, 39) define 12 different spatio-spectral patterns which are observable in all tasks, with more than 89% of subjects from each dataset present within each cluster. In general, these spatio-spectral maps appear consistent with maps generated in previous studies (Bridwell et al. 2013, 2016) and appear biologically plausible, demonstrating power within characteristic EEG frequency bands.

The spatio-spectral pattern in cluster 27 appears to capture eye artifacts, with peak values appearing over frontal electrodes. This cluster may have separated from cluster 17 likely due to different EEG preprocessing steps (i.e.

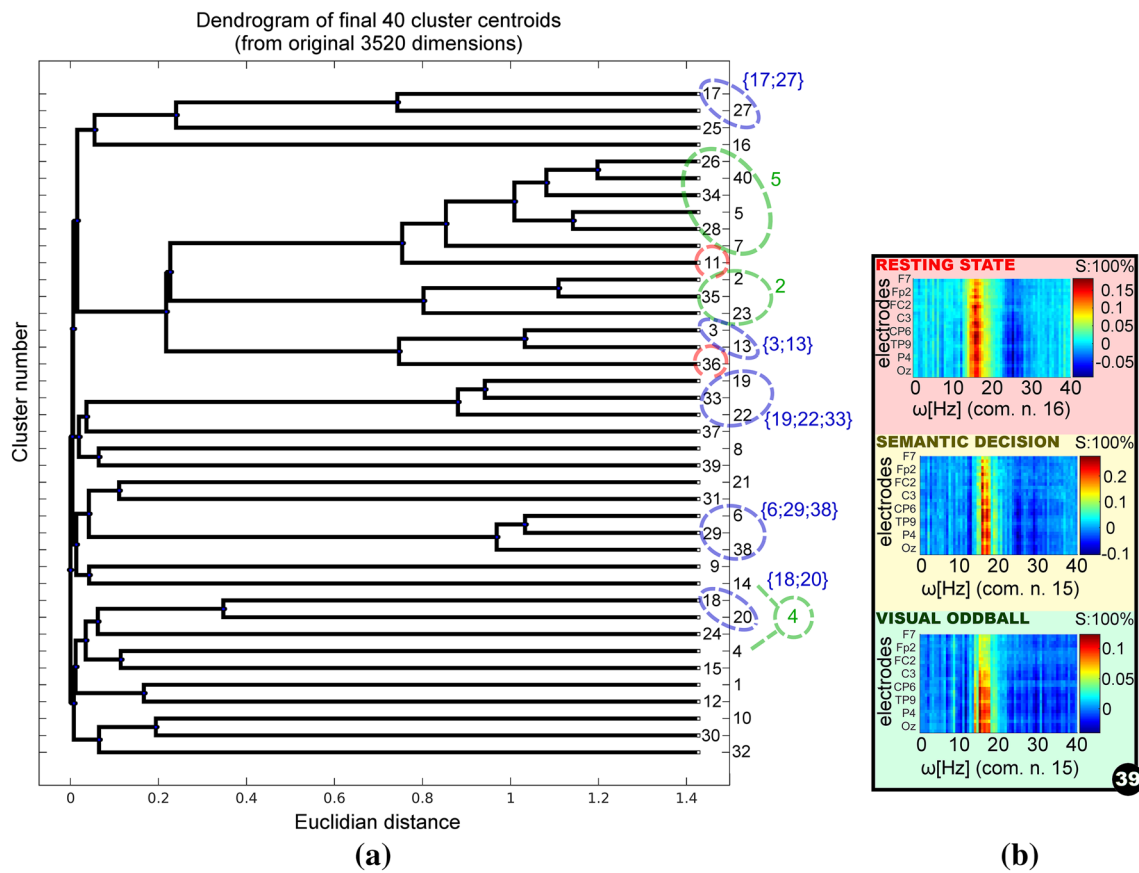


Fig. 3 Dendrogram of 40 clusters generated from k-means clustering (a) and cluster 39 as a representative example (b). (a) The green-circled clusters are the clusters combined during post-processing described within the Materials and Methods. The blue-circled clusters are the clusters which were not combined in post-processing, but were combined post hoc based upon visual inspection of the spatio-spectral patterns. The red-circled clusters are residuals which account for less than 5% of the single-subject spatio-spectral patterns within

any experimental paradigm. In (b), the spatio-spectral patterns were averaged for each experimental paradigm and cluster. The number on the upper right (e.g. “S:”) indicates the percentage of subjects who belong to the cluster. The spatial distribution of electrodes in each plot is: F7, F3, Fp1, Fz, Fp2, F4, F8, FC6, FC2, FC1, FC5, T7, C3, Cz, C4, T8, CP6, CP2, CP1, CP5, TP9, P7, P3, Pz, P4, P8, TP10, O2, Oz, O1

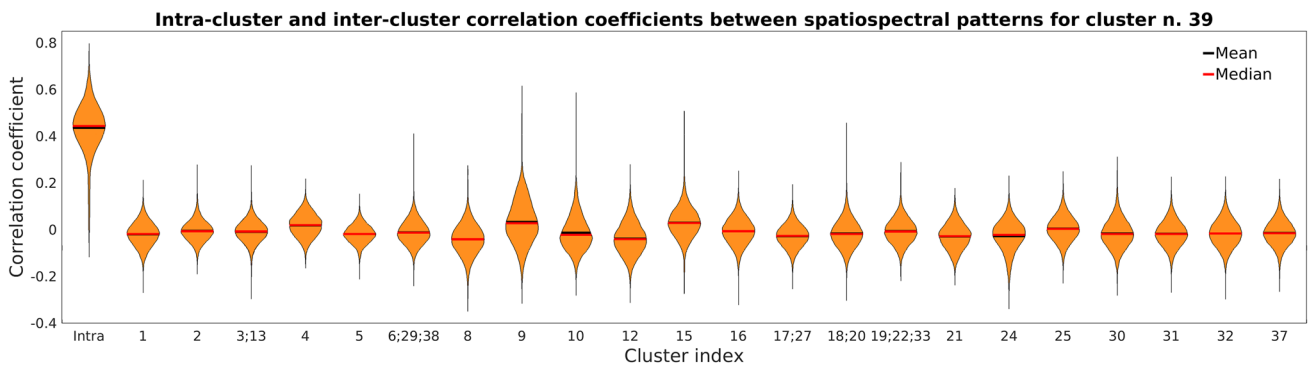


Fig. 4 K-means intra-cluster and inter-cluster correlation coefficients for cluster n. 39. Correlations between spatio-spectral patterns within cluster 39 were computed (e.g. intra-cluster correlations), and correlations between the patterns in cluster 39 and the patterns within the other clusters were computed (e.g. inter-cluster correlations) across the patterns for each subject, session, and paradigm pair. The violin plots indicate the distribution of intra-cluster correlations (leftmost plot) and the 22 distributions of inter-cluster correlations (i.e. the dis-

tribution of correlations between the patterns of cluster 39 patterns and the patterns within the other clusters, as indicated on the x-axis). The individual intra-cluster correlations were significantly larger than zero ($t=21.67$; $p=2.2 \times 10^{-16}$), and the inter-cluster correlations did not statistically differ for any of the 22 distributions computed (see Fig. 5). Results within this representative pattern indicate higher correlations within clusters than between clusters

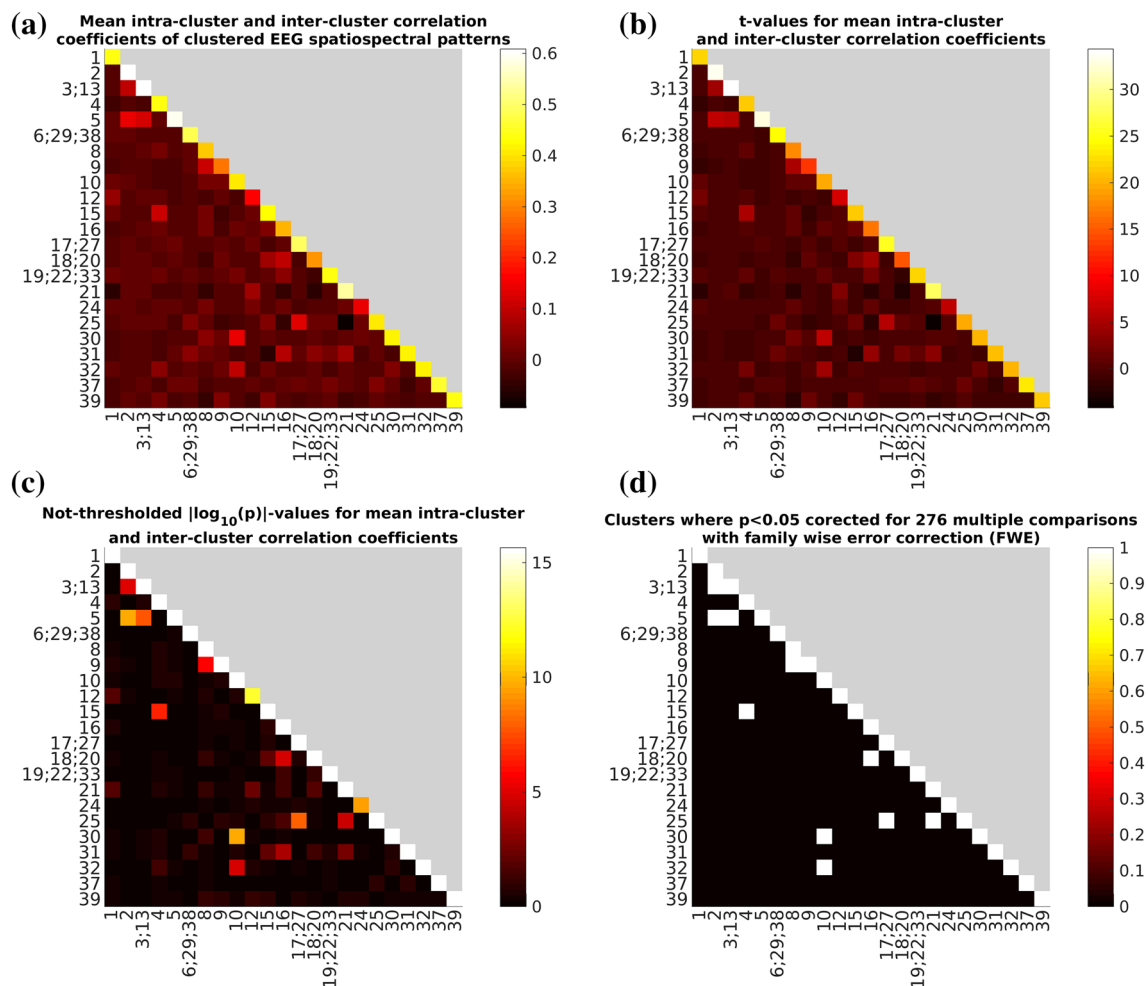


Fig. 5 Mean intra-cluster (*main diagonal*) and inter-cluster (*below the main diagonal*) correlation coefficients (a) over the final k-means clusters, the probabilities [the p values (c), derived from correlations coefficients through t-values (b)] indicating the likelihood that the

observed correlations differed from zero by chance and the supra-thresholded $p_{FWE} < 0.05$ (d). The labels indicate the final cluster indexes (see Fig. 3a)

eye-blink artifact correction applied to VOT but not RST-eye-closed or SDT data). Clusters number 1 and 12 consist of components with maximal narrow-band power slightly above 30 Hz, and cluster 24 appears to comprise a collection of residual (i.e. unique) spatio-spectral patterns.

Two spatio-spectral patterns which are observable in all datasets were divided at six disjunctive clusters where each cluster belongs to one specific dataset. On both the standard dendrogram (Fig. 3a) and the radial dendrogram projection (Fig. 6), these clusters form 2 different but neighboring groups and each group corresponds to a unique spatio-spectral pattern (cl. numbers {6;29;38} and {19;22;33}).

As demonstrated in Fig. 6, 21 of 30 clusters characterize 14 different spatio-spectral patterns which are observable and relatively stable in all three datasets. For exceptions, we note that clusters 25 and 31 contain some spatio-spectral patterns

which are present only during task, while the patterns of clusters 10 and 15 were present only during “rest”.

Relationship Between EEG Spatio-spectral Patterns and Stimulus

Statistical relationships between spatio-spectral time courses and stimulus vectors were present only at an uncorrected level of $p < 0.05$ (i.e. $\text{abs}(t \text{ value}) > 2.1$) for a subset of clusters and paradigms. None of the tests reached statistical significance using conservative corrections for multiple comparisons. Thus, it is likely that the dynamics of EEG’s spatio-spectral patterns are a mixture of the task-evoked neuronal activity and neuronal activity of task unrelated process (e.g. default mode activity).

In general, the majority of uncorrected statistical effects appear for the VOT (higher t-values for 8 patterns from 20

Table 1 Percentage of subjects belonging to the cluster within each dataset. If the cluster contained more components for one experimental paradigm, there are more values for one experiment

Cl. n.	RST (%)	SDT (%)	VOT (%)	PN
1	0	0	100	1
2	100	100	100	3
3;13	98	98	96	3
4	100	100	100	3
5	90	98	89	3
6;29;38	100	98	94	3
8	100	100	39	3
9	100	100	89	3
			73	
10	100	0	16	1
12	100	100	0	2
		98		
15	100	0	0	1
16	98	100	100	3
17;27	100	98	99	3
18;20	100	100	100	3
19;22;33	100	98	100	3
21	100	0	0	1
24	100	100	96	3
			51	
25	0	100	100	2
30	100	100	100	3
31	0	100	100	2
32	100	100	100	3
37	100	100	100	3
39	100	100	100	3

Cl. n. cluster number, RST resting-state, SDT semantic decision task, VOT visual oddball task, PN number of paradigms where the spatio-spectral pattern was observed

different clusters) than for the SDT (higher t-values only for 2 patterns from 20 different clusters).

Discussion

Stable EEG Spatospectral Patterns

EEG oscillations are often subdivided into distinct frequency bands which appear to represent distinct cognitive states (δ :0–4Hz, θ :4–8Hz, α :8–12Hz, β :12–20Hz and γ > 20 Hz) (Buzsaki 2006; Niedermeyer and da Silva 2011). Our results suggest that those bands can be further subdivided by frequency and electrode with data-driven group decomposition of independent spatospectral patterns, and that these patterns are stable across experimental paradigms.

Using the current approach, (i.e. with a high model order), we demonstrate a more detailed parcellation of

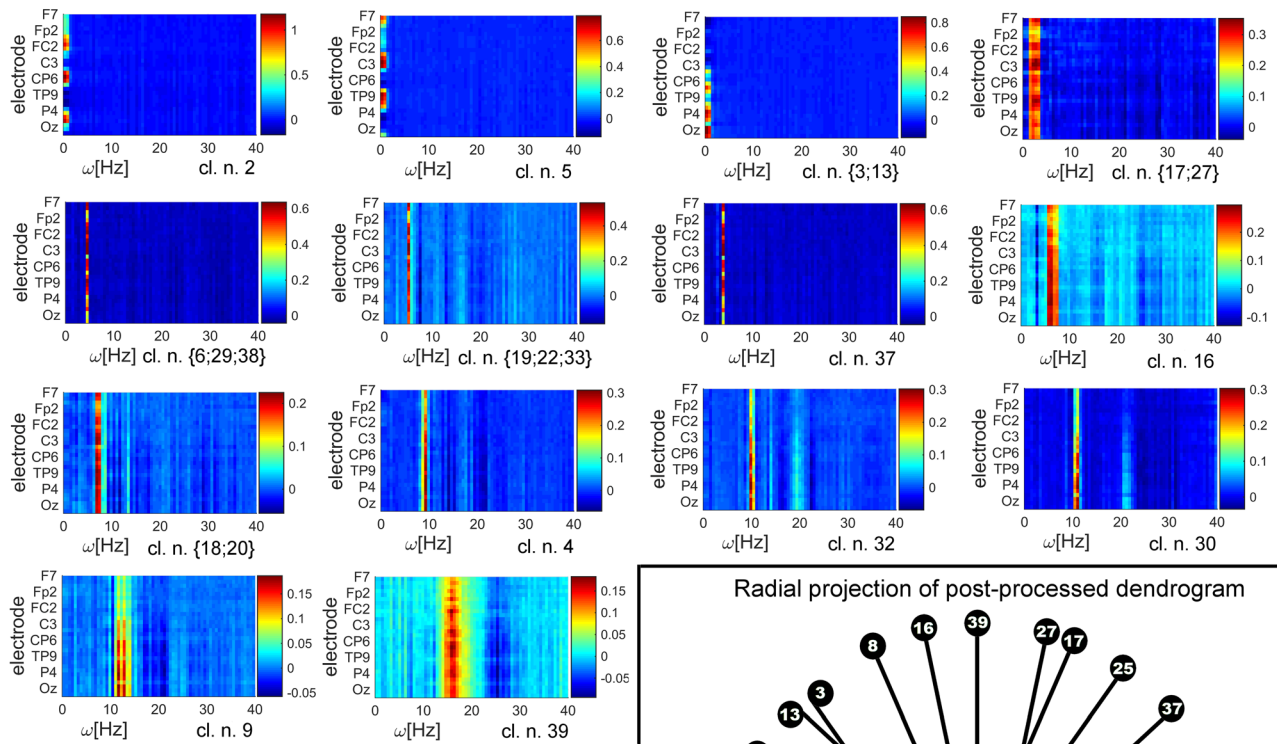
EEG sub-bands. The δ -band appears to have four independent spatospectral components (clusters 2, 5, {3;13} and {17;27}). The θ -band was divided into four stable independent mostly narrow-band clusters ({29;38;6}, {22;33;6}, 16; 37). The maximal α -band power was observed for three independent spatospectral patterns (cl. 4, 30 and 32). The stable β -band components converged into two clusters (9 and 39), and broad-band components within the γ -band were only observed within cluster {1;12}. The narrow-band components within the γ -band are likely non-neural in origin, potentially reflecting residual artifacts from the fMRI environment, as in (Mareček et al. 2016). In general, previous studies demonstrate that some EEG sub-bands differ with respect to their relationship to BOLD-fMRI (Laufs et al. 2006; Bridwell et al. 2013) and further studies may disentangle their potentially distinct relationships to cognition, and whether they are present to differing degrees within healthy and clinical populations.

The number components observed within each frequency band may depend on the model order (i.e. number of components) in ICA decomposition. For example, a given component may split into multiple components with a higher model order. The number of reliable components provides a useful metric for the appropriate choice of model order, since additional components are less reliably estimated when the model order is too high (Li et al. 2007). The model orders used within the present study appear appropriate, since cluster quality values are generally above 0.9, and were never below 0.7.

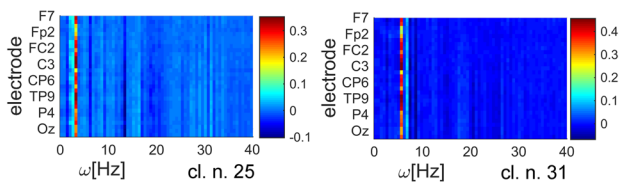
Although the subjects' groups partially overlapped for the SDT and RST datasets, the results indicate that the spatospectral patterns should be stable also over subjects. This conclusion is supported by three facts. First, the percentile of subjects belonging to the stable cluster is over 90% on average for all paradigms. Second, the VOT data involved totally disjunctive group of subjects from both other datasets. Third, the back-reconstruction of single-subject spatospectral patterns brings inter-subject variability into the k-means clustering analysis, which reorganizes the variability back into relevant, convergent and compact clusters.

Cortical oscillations may be tightly coupled with task dynamics, or may appear broadly throughout the task without a direct relationship to task parameters. For example, while we failed to identify robust relationships between spatospectral time courses and stimulus time courses, we have observed a few clusters which appear specific to the different experimental paradigms. For example, cluster numbers 25 and 31 were comprised of spatospectral maps which appeared during the two tasks, but not during rest (Fig. 6) and without a significant

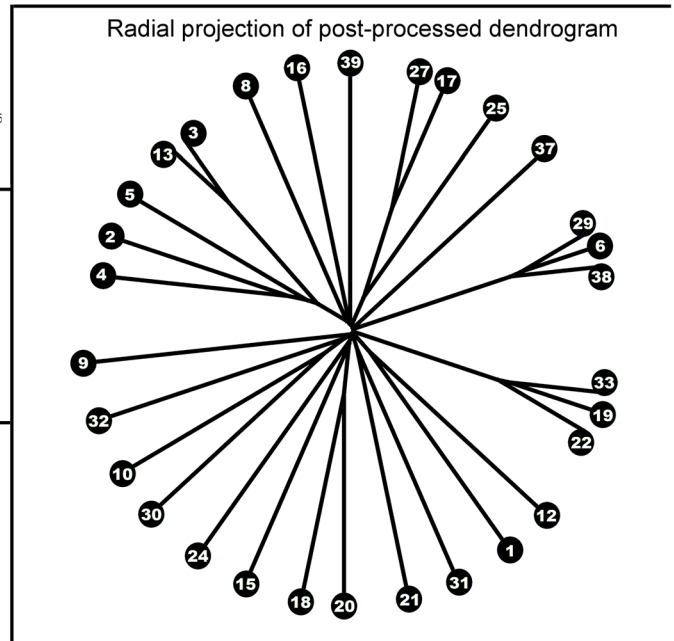
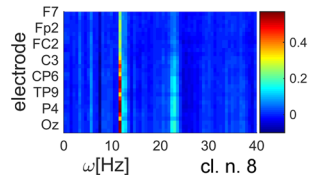
14 EEG spatospectral patterns stable over all paradigms



2 EEG spatospectral patterns stable over SDT and VOT



1 EEG spatospectral pattern stable over RST and SDT



Spatiospectral patterns stable over single paradigm (3 left patterns - RST, 1 right pattern VOT)

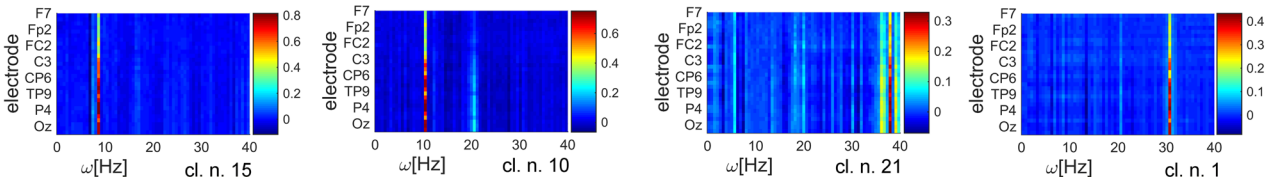


Fig. 6 Representative EEG spatospectral patterns for 28 of 30 final post-processed clusters stable over all, or over a subset paradigms; and radial projection of the post-processed dendrogram. Clusters 12

and 24 (within Fig. S5) are not included since their patterns appeared inconsistent across paradigms

relationship to stimuli timings. This finding suggests that these networks emerge or support cognitive processes utilized during visual oddball or semantic decision tasks, but they are unrelated to the stimulus time courses directly (e.g. representing arousal).

Spatiospectral Pattern Dynamics and External Stimulation

Relationships between spatio-spectral fluctuations and the stimulus timing failed to reach statistical significance after correcting for multiple comparisons, despite previous studies demonstrating relationships between spectra and tasks (Rosa et al. 2010; Yuan et al. 2010; Miller 2010; Sclocco et al. 2014). Our previous study demonstrated stronger associations with power fluctuations and VOT stimuli (Labounek et al. 2015), consistent with the notion that relative EEG power contains more task-related variability than absolute EEG power (Klimesch 1999; Kilner et al. 2005). However, while relative power could increase task-related variability in the output W matrices of spatio-spectral group ICA (Labounek et al. 2016) a decrease in the cluster quality of S matrix estimates is observed (Fig. S6–8). It is also possible that task dynamics may have been attenuated within the present study as a result of the PCA dimension reduction. The PCA reduction of aggregate group data potentially emphasizes the most powerful and robust EEG spatio-spectral maps (e.g. ongoing low frequency oscillations), reducing the influence of task specific activities that represent only a small portion of signal variance, such as high frequency gamma band activity or event-related potentials (ERPs). In addition, it is important to note that the present approach isolates EEG responses over large windows (e.g. 1.66 s in the present study), which discards the time-locked activity present with conventional Event-Related Potential (ERP) analysis of task data. Preserving time-locked activity, e.g. with group temporal ICA, may be a more promising approach for task data.

The stable spatio-spectral maps observed within the present study may be related to network activity that contributes to large scale brain networks (LSBNs) reported in “resting-state” fMRI studies (Damoiseaux et al. 2006; Van Den Heuvel et al. 2009; Allen et al. 2011), LSBNs have been observed during tasks, their activity sometimes covaries with the experimental time course (Calhoun et al. 2008; Mantini et al. 2009; Spadone et al. 2015), and sub-set of LSBNs are related to EEG power fluctuations in concurrently recorded EEG (Mantini et al. 2007; Bridwell et al. 2013; Mareček et al. 2016, 2017; for review see Bridwell and Calhoun 2014; or Murta et al. 2015). Thus, an improved understanding of the stable spatio-spectral patterns may lead

to and improved understanding of LSBNs observed with fMRI.

Current Study Novelty, Limits and Future Work

To the best of our knowledge, the present manuscript is the first to demonstrate the stability of EEG independent spatio-spectral patterns over different datasets. These findings further validate the approach for future studies, and motivate investigation of the functional role of the distinct spatio-spectral patterns. Subdividing spectral responses in a data driven manner will be useful for future studies that decompose separate signals with potentially distinct functional roles (i.e. generating more robust results) and separating signals from artifact (i.e. enhancing signal over noise).

These stable patterns may be useful for brain computer interface (BCI) research (Wolpaw et al. 2000), since EEG spatio-spectral filters are often applied as an approach to denoise the data (Lemm et al. 2005; Dornhege et al. 2006; Tomioka et al. 2006; Novi et al. 2007; Ang et al. 2008; Wu et al. 2008; Meng et al. 2013). The approach may also be useful in clinical research and applications focused on spectral differences between populations within distinct frequency bands, e.g. as demonstrated for Alzheimer’s (Rodriguez et al. 1999; Jeong 2004) or Parkinson’s (Soikeli et al. 1991; Klassen et al. 2011) diseases. If the stability issues with relative EEG power were minimized, Group ICA may also be useful for examining the relative power differences prominent in autism (Wang et al. 2015).

It is unclear why we were unable to observe biologically plausible components within the γ -band within the present study, since previous studies demonstrate correlations between γ -band and BOLD signals during tasks (Foucher et al. 2003; Lachaux et al. 2007; Nir et al. 2007; Scheeringa et al. 2011), and due to its association with perception and feature binding (Fries et al. 2007). Since Infomax ICA emphasizes sparse independent components (Calhoun et al. 2013), it’s possible that the component histograms within the present study differed due to the number of electrodes or by the choice of bin size (dictated by the window size), modulating the sparsity and independence of γ -band components such that they were difficult to decompose. This frequency range may be more influenced by these parameters, thus, further studies focusing on this frequency band may use parameters more consistent with previous studies. In addition, results may improve after introducing overlap between the EEG segments (Bridwell et al. 2016).

Finally, future research could compare the consistency of group results derived using other approaches that generate EEG spatio-spectral patterns, such as group-clustering after single-subject ICA (Hyvärinen 2011; Hyvärinen and

Ramkumar 2013), approximate joint diagonalization of lagged-covariance (Tang et al. 2005) or cospectral matrices (Congedo et al. 2008, 2010).

Acknowledgements We would like to thank Dr. Milena Košťálová for her help with designing the semantic decision task. This research was supported Grant No. P304/11/1318 of Grant Agency of Czech Republic, by Grants Nos. FEKT-S-14-2210 and FEKT-S-11-2-921 of Brno University of Technology, by Grants Nos. CZ.1.05/1.1.00/02.0068 of Central European Institute of Technology and by Grants Nos. AZV 16-302100A of Palacký University. The funding is highly acknowledged. Computational resources were provided by the MetaCentrum under the program LM2010005 and the CERIT-SC under the program Centre CERIT Scientific Cloud, part of the Operational Program Research and Development for Innovations, Reg. No. CZ.1.05/3.2.00/08.0144.

References

- Allen PJ, Polizzi G, Krakow K et al (1998) Identification of EEG events in the MR scanner: the problem of pulse artifact and a method for its subtraction. *Neuroimage* 8:229–239. doi: [10.1006/nimg.1998.0361](https://doi.org/10.1006/nimg.1998.0361)
- Allen PJ, Josephs O, Turner R (2000) A method for removing imaging artifact from continuous EEG recorded during functional MRI. *Neuroimage* 12:230–239. doi: [10.1006/nimg.2000.0599](https://doi.org/10.1006/nimg.2000.0599)
- Allen EA, Erhardt EB, Damaraju E et al (2011) A baseline for the multivariate comparison of resting-state networks. *Front Syst Neurosci* 5:2. doi: [10.3389/fnsys.2011.00002](https://doi.org/10.3389/fnsys.2011.00002)
- Allen EA, Erhardt EB, Wei Y et al (2012) Capturing inter-subject variability with group independent component analysis of fMRI data: a simulation study. *Neuroimage* 59:4141–4159. doi: [10.1016/j.neuroimage.2011.10.010](https://doi.org/10.1016/j.neuroimage.2011.10.010)
- Anemüller J, Sejnowski TJ, Makeig S (2003) Complex independent component analysis of frequency-domain electroencephalographic data. *Neural Netw* 16:1311–1323. doi: [10.1016/j.neunet.2003.08.003](https://doi.org/10.1016/j.neunet.2003.08.003)
- Ang KK, Chin ZY, Zhang H, Guan C (2008) Filter Bank Common Spatial Pattern (FBCSP) in Brain-Computer Interface. *Int Jt Conf Neural Networks*. doi: [10.1109/IJCNN.2008.4634130](https://doi.org/10.1109/IJCNN.2008.4634130)
- Bell AJ, Sejnowski TJ (1995) An information-maximization approach to blind separation and blind deconvolution. *Neural Comput* 7:1129–1159. doi: [10.1162/neco.1995.7.6.1129](https://doi.org/10.1162/neco.1995.7.6.1129)
- Belouchrani A, Abed-Meraim K, Cardoso JF, Moulines E (1997) A blind source separation technique using second-order statistics. *IEEE Trans Signal Process* 45:434–444. doi: [10.1109/78.554307](https://doi.org/10.1109/78.554307)
- Bernat EM, Williams WJ, Gehring WJ (2005) Decomposing ERP time-frequency energy using PCA. *Clin Neurophysiol* 116:1314–1334. doi: [10.1016/j.clinph.2005.01.019](https://doi.org/10.1016/j.clinph.2005.01.019)
- Brázdil M, Mikl M, Mareček R et al (2007) Effective connectivity in target stimulus processing: a dynamic causal modeling study of visual oddball task. *Neuroimage* 35:827–835. doi: [10.1016/j.neuroimage.2006.12.020](https://doi.org/10.1016/j.neuroimage.2006.12.020)
- Bridwell DA, Calhoun V (2014) Fusing Concurrent EEG and fMRI intrinsic networks. In: *Magnetoencephalography*. Springer, Berlin Heidelberg, pp 213–235
- Bridwell DA, Wu L, Eichele T, Calhoun VD (2013) The spatio-spectral characterization of brain networks: fusing concurrent EEG spectra and fMRI maps. *Neuroimage* 69:101–111. doi: [10.1016/j.neuroimage.2012.12.024](https://doi.org/10.1016/j.neuroimage.2012.12.024)
- Bridwell DA, Kiehl KA, Pearson GD, Calhoun VD (2014) Patients with schizophrenia demonstrate reduced cortical sensitivity to auditory oddball regularities. *Schizophr Res* 158:189–194. doi: [10.1016/j.schres.2014.06.037](https://doi.org/10.1016/j.schres.2014.06.037)
- Bridwell DA, Steele VR, Maurer JM et al (2015) The relationship between somatic and cognitive-affective depression symptoms and error-related ERPs. *J Affect Disord* 172:89–95. doi: [10.1016/j.jad.2014.09.054](https://doi.org/10.1016/j.jad.2014.09.054)
- Bridwell DA, Rachakonda S, Silva RF et al (2016) Spatio-spectral decomposition of multi-subject eeg: evaluating blind source separation algorithms on real and realistic simulated data. *Brain Topogr*. doi: [10.1007/s10548-016-0479-1](https://doi.org/10.1007/s10548-016-0479-1)
- Buzsáki G (2006) *Rhythms of the Brain*. Oxford University Press, Oxford
- Calhoun VD, Adalı T (2012) Multisubject independent component analysis of fMRI: a decade of intrinsic networks, default mode, and neurodiagnostic discovery. *IEEE Rev Biomed Eng* 5:60–73. doi: [10.1109/RBME.2012.2211076](https://doi.org/10.1109/RBME.2012.2211076)
- Calhoun VD, Adalı T, Pearson GD, Pekar JJ (2001) A method for making group inferences from functional mri data using independent component analysis. *Hum Brain Mapp* 14:140–151. doi: [10.1002/hbm](https://doi.org/10.1002/hbm)
- Calhoun VD, Pekar JJ, Pearson GD (2004) Alcohol intoxication effects on simulated driving: exploring alcohol-dose effects on brain activation using functional MRI. *Neuropsychopharmacology* 29:2097–2107. doi: [10.1038/sj.npp.1300543](https://doi.org/10.1038/sj.npp.1300543)
- Calhoun VD, Kiehl KA, Pearson GD (2008) Modulation of temporally coherent brain networks estimated using ICA at rest and during cognitive tasks. *Hum Brain Mapp* 29:828–838. doi: [10.1002/hbm.20581](https://doi.org/10.1002/hbm.20581)
- Calhoun VD, Potluru VK, Phlypo R et al (2013) Independent component analysis for brain fMRI does indeed select for maximal independence. *PLoS ONE* 8:1–8. doi: [10.1371/journal.pone.0073309](https://doi.org/10.1371/journal.pone.0073309)
- Cong F, He Z, Hämäläinen J et al (2013) Validating rationale of group-level component analysis based on estimating number of sources in EEG through model order selection. *J Neurosci Methods* 212:165–172. doi: [10.1016/j.jneumeth.2012.09.029](https://doi.org/10.1016/j.jneumeth.2012.09.029)
- Congedo M, Gouy-Pailler C, Jutten C (2008) On the blind source separation of human electroencephalogram by approximate joint diagonalization of second order statistics. *Clin Neurophysiol* 119:2677–2686. doi: [10.1016/j.clinph.2008.09.007](https://doi.org/10.1016/j.clinph.2008.09.007)
- Congedo M, John RE, De Ridder D, Prichep L (2010) Group independent component analysis of resting state EEG in large normative samples. *Int J Psychophysiol* 78:89–99. doi: [10.1016/j.ijpsycho.2010.06.003](https://doi.org/10.1016/j.ijpsycho.2010.06.003)
- Damoiseaux JS, Rombouts SAR, Barkhof F et al (2006) Consistent resting-state networks across healthy subjects. *Proc Natl Acad Sci USA* 103:13848–13853. doi: [10.1073/pnas.0601417103](https://doi.org/10.1073/pnas.0601417103)
- Dornhege G, Blankertz B, Krauledat M et al (2006) Combined optimization of spatial and temporal filters for improving brain-computer interfacing. *IEEE Trans Biomed Eng* 53:2274–2281. doi: [10.1109/TBME.2006.883649](https://doi.org/10.1109/TBME.2006.883649)
- Doron E, Yeredor A (2004) Asymptotically optimal blind separation of parametric Gaussian sources. In: *Independent component analysis and blind signal separation*. Springer, Berlin, Heidelberg, pp 390–397
- Eichele T, Rachakonda S, Brakedal B et al (2011) EEGIFT: Group independent component analysis for event-related EEG data. *Comput Intell Neurosci*. doi: [10.1155/2011/129365](https://doi.org/10.1155/2011/129365)
- Erhardt EB, Rachakonda S, Bedrick EJ et al (2011) Comparison of multi-subject ICA methods for analysis of fMRI data. *Hum Brain Mapp* 32:2075–2095. doi: [10.1002/hbm.21170](https://doi.org/10.1002/hbm.21170)
- Foucher JR, Otzenberger H, Gounot D (2003) The BOLD response and the gamma oscillations respond differently than evoked potentials: an interleaved EEG-fMRI study. *Neuroscience* 4:1–11. doi: [10.1186/1471-2202-4-22](https://doi.org/10.1186/1471-2202-4-22)

- Fries P, Nikolicić D, Singer W (2007) The gamma cycle. *Trends Neurosci* 30:309–316. doi: [10.1016/j.tins.2007.05.005](https://doi.org/10.1016/j.tins.2007.05.005)
- Friston KJ, Holmes AP, Worsley KJ et al (1994) Statistical parametric maps in functional imaging: a general linear approach. *Hum Brain Mapp* 2:189–210. doi: [10.1002/hbm.460020402](https://doi.org/10.1002/hbm.460020402)
- Himberg J, Hyvärinen A (2003) Icasto: software for investigating the reliability of ICA estimates by clustering and visualization. In: 13th Workshop on Neural Networks for Signal Processing. IEEE, pp 259–268
- Himberg J, Hyvärinen A, Esposito F (2004) Validating the independent components of neuroimaging time series via clustering and visualization. *Neuroimage* 22:1214–1222. doi: [10.1016/j.neuroimage.2004.03.027](https://doi.org/10.1016/j.neuroimage.2004.03.027)
- Hu L, Zhang ZG, Mouraux A, Iannetti GD (2015) Multiple linear regression to estimate time-frequency electrophysiological responses in single trials. *Neuroimage* 111:442–453. doi: [10.1016/j.neuroimage.2015.01.062](https://doi.org/10.1016/j.neuroimage.2015.01.062)
- Huster RJ, Plis SM, Calhoun VD (2015) Group-level component analyses of EEG: validation and evaluation. *Front Neurosci* 9:254. doi: [10.3389/fnins.2015.00254](https://doi.org/10.3389/fnins.2015.00254)
- Hyvärinen A (2011) Testing the ICA mixing matrix based on inter-subject or inter-session consistency. *Neuroimage* 58:122–136. doi: [10.1016/j.neuroimage.2011.05.086](https://doi.org/10.1016/j.neuroimage.2011.05.086)
- Hyvärinen A, Ramkumar P (2013) Testing independent component patterns by inter-subject or inter-session consistency. *Front Hum Neurosci* 7:94. doi: [10.3389/fnhum.2013.00094](https://doi.org/10.3389/fnhum.2013.00094)
- Hyvärinen A, Karhunen J, Oja E (2001) Independent component analysis. Wiley, New York
- Hyvärinen A, Ramkumar P, Parkkonen L, Hari R (2010) Independent component analysis of short-time Fourier transforms for spontaneous EEG/MEG analysis. *Neuroimage* 49:257–271. doi: [10.1016/j.neuroimage.2009.08.028](https://doi.org/10.1016/j.neuroimage.2009.08.028)
- Jeong J (2004) EEG dynamics in patients with Alzheimer's disease. *Clin Neurophysiol* 115:1490–1505. doi: [10.1016/j.clinph.2004.01.001](https://doi.org/10.1016/j.clinph.2004.01.001)
- Kauppi JP, Parkkonen L, Hari R, Hyvärinen A (2013) Decoding magnetoencephalographic rhythmic activity using spectrospatial information. *Neuroimage* 83:921–936. doi: [10.1016/j.neuroimage.2013.07.026](https://doi.org/10.1016/j.neuroimage.2013.07.026)
- Kilner JMM, Mattout J, Henson R, Friston KJ (2005) Hemodynamic correlates of EEG: a heuristic. *Neuroimage* 28:280–286. doi: [10.1016/j.neuroimage.2005.06.008](https://doi.org/10.1016/j.neuroimage.2005.06.008)
- Klassen BT, Hentz JG, Shill HA et al (2011) Quantitative EEG as a predictive biomarker for Parkinson disease dementia. *Neurology* 77:118–124. doi: [10.1212/WNL.0b013e318224af8d](https://doi.org/10.1212/WNL.0b013e318224af8d)
- Klimesch W (1999) EEG alpha and theta oscillations reflect cognitive and memory performance: a review and analysis. *Brain Res Rev* 29:169–195. doi: [10.1016/S0165-0173\(98\)00056-3](https://doi.org/10.1016/S0165-0173(98)00056-3)
- Kovacevic N, McIntosh AR (2007) Groupwise independent component decomposition of EEG data and partial least square analysis. *Neuroimage* 35:1103–1112. doi: [10.1016/j.neuroimage.2007.01.016](https://doi.org/10.1016/j.neuroimage.2007.01.016)
- Labounek R, Lamoš M, Mareček R et al (2015) Exploring task-related variability in fMRI data using fluctuations in power spectrum of simultaneously acquired EEG. *J Neurosci Methods* 245:125–136. doi: [10.1016/j.jneumeth.2015.02.016](https://doi.org/10.1016/j.jneumeth.2015.02.016)
- Labounek R, Janeček D, Mareček R et al (2016) Generalized EEG-fMRI spectral and spatio-spectral heuristic models. In: IEEE 13th international symposium on biomedical imaging: From nano to macro. IEEE, Prague, pp 767–770. doi: [10.1109/ISBI.2016.7493379](https://doi.org/10.1109/ISBI.2016.7493379)
- Lachaux J-P, Fonlupt P, Kahane P et al (2007) Relationship between task-related gamma oscillations and BOLD signal: New insights from combined fMRI and intracranial EEG. *Hum Brain Mapp* 28:1368–1375. doi: [10.1002/hbm.20352](https://doi.org/10.1002/hbm.20352)
- Laufs H, Holt JL, Elfont R et al (2006) Where the BOLD signal goes when alpha EEG leaves. *Neuroimage* 31:1408–1418. doi: [10.1016/j.neuroimage.2006.02.002](https://doi.org/10.1016/j.neuroimage.2006.02.002)
- Lemm S, Blankertz B, Curio G, Müller KR (2005) Spatio-spectral filters for improving the classification of single trial EEG. *IEEE Trans Biomed Eng* 52:1541–1548. doi: [10.1109/TBME.2005.851521](https://doi.org/10.1109/TBME.2005.851521)
- Li Y-O, Adali T, Calhoun VD (2007) Estimating the number of independent components for functional magnetic resonance imaging data. *Hum Brain Mapp* 28:1251–1266. doi: [10.1002/hbm.20359](https://doi.org/10.1002/hbm.20359)
- Li S, Wang Y, Bin G et al (2015) Space distribution of EEG responses to hanoi-moving visual and auditory stimulation with fourier independent component analysis. *Front Hum Neurosci* 9:1–13. doi: [10.3389/fnhum.2015.00405](https://doi.org/10.3389/fnhum.2015.00405)
- Lio G, Boulinguez P (2013) Greater robustness of second order statistics than higher order statistics algorithms to distortions of the mixing matrix in blind source separation of human EEG: implications for single-subject and group analyses. *Neuroimage* 67:137–152. doi: [10.1016/j.neuroimage.2012.11.015](https://doi.org/10.1016/j.neuroimage.2012.11.015)
- Makeig S, Jung TP, Bell AJ et al (1997) Blind separation of auditory event-related brain responses into independent components. *Proc Natl Acad Sci USA* 94:10979–10984. doi: [10.1073/pnas.94.20.10979](https://doi.org/10.1073/pnas.94.20.10979)
- Makeig S, Debener S, Onton J, Delorme A (2004) Mining event-related brain dynamics. *Trends Cogn Sci* 8:204–210. doi: [10.1016/j.tics.2004.03.008](https://doi.org/10.1016/j.tics.2004.03.008)
- Mantini D, Perrucci MG, Del Gratta C et al (2007) Electrophysiological signatures of resting state networks in the human brain. *Proc Natl Acad Sci USA* 104:13170–13175. doi: [10.1073/pnas.0700668104](https://doi.org/10.1073/pnas.0700668104)
- Mantini D, Corbetta M, Perrucci MG et al (2009) Large-scale brain networks account for sustained and transient activity during target detection. *Neuroimage* 44:265–274. doi: [10.1016/j.neuroimage.2008.08.019](https://doi.org/10.1016/j.neuroimage.2008.08.019)
- Mareček R, Lamoš M, Mikl M et al (2016) What can be found in scalp EEG spectrum beyond common frequency bands. EEG-fMRI study. *J Neural Eng* 13:1–13. doi: [10.1088/1741-2560/13/4/046026](https://doi.org/10.1088/1741-2560/13/4/046026)
- Mareček R, Lamoš M, Labounek R et al (2017) Multiway array decomposition of EEG spectrum: Implications of its stability for the exploration of large-scale brain networks. *Neural Comput*. doi: [10.1162/NECO_a_00933](https://doi.org/10.1162/NECO_a_00933)
- Meng J, Huang G, Zhang D, Zhu X (2013) Optimizing spatial spectral patterns jointly with channel configuration for brain-computer interface. *Neurocomputing* 104:115–126. doi: [10.1016/j.neucom.2012.11.004](https://doi.org/10.1016/j.neucom.2012.11.004)
- Miller KJ (2010) Broadband spectral change: evidence for a macroscale correlate of population firing rate? *J Neurosci* 30:6477–6479. doi: [10.1523/JNEUROSCI.6401-09.2010](https://doi.org/10.1523/JNEUROSCI.6401-09.2010)
- Murta T, Leite M, Carmichael DW et al (2015) Electrophysiological correlates of the BOLD signal for EEG-informed fMRI. *Hum Brain Mapp* 36:391–414. doi: [10.1002/hbm.22623](https://doi.org/10.1002/hbm.22623)
- Niedermeyer E, da Silva FL (2011) Electroencephalography: basic principles, clinical applications, and related fields, 6th edn. Lippincott Williams & Wilkins, Philadelphia
- Nikulin VV, Nolte G, Curio G (2011) A novel method for reliable and fast extraction of neuronal EEG/MEG oscillations on the basis of spatio-spectral decomposition. *Neuroimage* 55:1528–1535. doi: [10.1016/j.neuroimage.2011.01.057](https://doi.org/10.1016/j.neuroimage.2011.01.057)
- Nir Y, Fisch L, Mukamel R et al (2007) Coupling between Neuronal Firing Rate, Gamma LFP, and BOLD fMRI is related to interneuronal correlations. *Curr Biol* 17:1275–1285. doi: [10.1016/j.cub.2007.06.066](https://doi.org/10.1016/j.cub.2007.06.066)
- Novi Q, Guan C, Dat TH, Xue P (2007) Sub-band common spatial pattern (SBCSP) for brain-computer interface. *Proc 3rd Int IEEE EMBS Conf Neural Eng*. doi: [10.1109/CNE.2007.369647](https://doi.org/10.1109/CNE.2007.369647)

- Nunez PL, Srinivasan R (2006) Electric fields of the brain: the neurophysics of EEG, 2nd edn. Oxford University Press, New York
- Onton J, Delorme A, Makeig S (2005) Frontal midline EEG dynamics during working memory. *Neuroimage* 27:341–356. doi: [10.1016/j.neuroimage.2005.04.014](https://doi.org/10.1016/j.neuroimage.2005.04.014)
- Onton J, Westerfield M, Townsend J, Makeig S (2006) Imaging human EEG dynamics using independent component analysis. *Neurosci Biobehav Rev* 30:808–822. doi: [10.1016/j.neubiorev.2006.06.007](https://doi.org/10.1016/j.neubiorev.2006.06.007)
- Pascual-Marqui RD, Michel CM, Lehmann D (1995) Segmentation of brain electrical activity into microstates: model estimation and validation. *Trans Biomed Eng IEEE* 42:658–665. doi: [10.1109/10.391164](https://doi.org/10.1109/10.391164)
- Ponomarev VA, Mueller A, Candrian G et al (2014) Group Independent Component Analysis (gICA) and Current Source Density (CSD) in the study of EEG in ADHD adults. *Clin Neurophysiol* 125:83–97. doi: [10.1016/j.clinph.2013.06.015](https://doi.org/10.1016/j.clinph.2013.06.015)
- Ramkumar P, Parkkonen L, Hari R, Hyvärinen A (2012) Characterization of neuromagnetic brain rhythms over time scales of minutes using spatial independent component analysis. *Hum Brain Mapp* 33:1648–1662. doi: [10.1002/hbm.21303](https://doi.org/10.1002/hbm.21303)
- Ramkumar P, Parkkonen L, Hyvärinen A (2014) Group-level spatial independent component analysis of Fourier envelopes of resting-state MEG data. *Neuroimage* 86:480–491. doi: [10.1016/j.neuroimage.2013.10.032](https://doi.org/10.1016/j.neuroimage.2013.10.032)
- Rodriguez G, Copello F, Vitali P et al (1999) EEG spectral profile to stage Alzheimer's disease. *Clin Neurophysiol* 110:1831–1837. doi: [10.1016/S1388-2457\(99\)00123-6](https://doi.org/10.1016/S1388-2457(99)00123-6)
- Rosa MJ, Kilner J, Blankenburg F et al (2010) Estimating the transfer function from neuronal activity to BOLD using simultaneous EEG-fMRI. *Neuroimage* 49:1496–1509. doi: [10.1016/j.neuroimage.2009.09.011](https://doi.org/10.1016/j.neuroimage.2009.09.011)
- Scheeringa RR, Fries P, Petersson K-MM et al (2011) Neuronal dynamics underlying high- and low-frequency EEG oscillations contribute independently to the human BOLD signal. *Neuron* 69:572–583. doi: [10.1016/j.neuron.2010.11.044](https://doi.org/10.1016/j.neuron.2010.11.044)
- Sclocco R, Tana MG, Visani E et al (2014) EEG-informed fMRI analysis during a hand grip task: estimating the relationship between EEG rhythms and the BOLD signal. *Front Hum Neurosci* 8:186. doi: [10.3389/fnhum.2014.00186](https://doi.org/10.3389/fnhum.2014.00186)
- Shou G, Ding L, Dasari D (2012) Probing neural activations from continuous EEG in a real-world task: Time-frequency independent component analysis. *J Neurosci Methods* 209:22–34. doi: [10.1016/j.jneumeth.2012.05.022](https://doi.org/10.1016/j.jneumeth.2012.05.022)
- Soikkeli R, Partanen J, Soininen H et al (1991) Slowing of EEG in Parkinson's disease. *Electroencephalogr Clin Neurophysiol* 79:159–165. doi: [10.1016/0013-4694\(91\)90134-P](https://doi.org/10.1016/0013-4694(91)90134-P)
- Spadone S, Della Penna S, Sestieri C et al (2015) Dynamic reorganization of human resting-state networks during visuospatial attention. *Proc Natl Acad Sci USA* 112:8112–8117. doi: [10.1073/pnas.1415439112](https://doi.org/10.1073/pnas.1415439112)
- Stone JV (2004) Independent component analysis: a tutorial introduction. MIT press, Cambridge
- Takeda Y, Hiroe N, Yamashita O, Sato M aki (2016) Estimating repetitive spatiotemporal patterns from resting-state brain activity data. *Neuroimage* 133:251–265. doi: [10.1016/j.neuroimage.2016.03.014](https://doi.org/10.1016/j.neuroimage.2016.03.014)
- Tang A (2010) Applications of second order blind identification to high-density EEG-based brain imaging: a review. In: International Symposium on Neural Networks. Springer Berlin, Heidelberg, pp 368–377
- Tang AC, Sutherland MT, McKinney CJ (2005) Validation of SOBI components from high-density EEG. *Neuroimage* 25:539–553. doi: [10.1016/j.neuroimage.2004.11.027](https://doi.org/10.1016/j.neuroimage.2004.11.027)
- Tichavský P, Koldovský Z, Doron E et al (2006) Blind signal separation by combining two ICA algorithms: HOS-based EFICA and time structure-based WASOBI. In: 14th European Signal Processing Conference. IEEE, Florence, pp 1–5
- Tomioka R, Dornhege G, Nolte G et al (2006) Spectrally weighted Common Spatial Pattern algorithm for single trial EEG classification. *Dept Math Eng Univ Tokyo Tokyo Japan Tech Rep* 40:1–23
- Van Den Heuvel MP, Mandl RCW, Kahn RS, Hulshoff Pol HE (2009) Functionally linked resting-state networks reflect the underlying structural connectivity architecture of the human brain. *Hum Brain Mapp* 30:3127–3141. doi: [10.1002/hbm.20737](https://doi.org/10.1002/hbm.20737)
- Van Der Meij R, Van Ede F, Maris E (2016) Rhythmic components in extracranial brain signals reveal multifaceted task modulation of overlapping neuronal activity. *PLoS ONE* 11:1–28. doi: [10.1371/journal.pone.0154881](https://doi.org/10.1371/journal.pone.0154881)
- Wang Y, Sokhadze EM, El-Baz AS et al (2015) Relative power of specific EEG bands and their ratios during neurofeedback training in children with autism spectrum disorder. *Front Hum Neurosci* 9:723. doi: [10.3389/fnhum.2015.00723](https://doi.org/10.3389/fnhum.2015.00723)
- Wolpaw JR, Birbaumer N, Heetderks WJ et al (2000) Brain-computer interface technology: a review of the first international meeting. *IEEE Trans Rehabil Eng* 8:164–173. doi: [10.1109/TRE.2000.847807](https://doi.org/10.1109/TRE.2000.847807)
- Wu W, Gao X, Hong B, Gao S (2008) Classifying single-trial EEG during motor imagery by iterative spatio-spectral patterns learning (ISSPL). *IEEE Trans Biomed Eng* 55:1733–1743. doi: [10.1109/TBME.2008.919125](https://doi.org/10.1109/TBME.2008.919125)
- Wu L, Eichele T, Calhoun VD (2010) Reactivity of hemodynamic responses and functional connectivity to different states of alpha synchrony: a concurrent EEG-fMRI study. *Neuroimage* 52:1252–1260. doi: [10.1016/j.neuroimage.2010.05.053](https://doi.org/10.1016/j.neuroimage.2010.05.053)
- Yeredor A (2000) Blind source separation via the second characteristic function. *Signal Process* 80:897–902. doi: [10.1016/S0165-1684\(00\)00062-1](https://doi.org/10.1016/S0165-1684(00)00062-1)
- Yu Q, Wu L, Bridwell DA et al (2016) Building an EEG-fMRI multimodal brain graph: a concurrent EEG-fMRI study. *Front Hum Neurosci*. doi: [10.3389/fnhum.2016.00476](https://doi.org/10.3389/fnhum.2016.00476)
- Yuan H, Liu T, Szarkowski R et al (2010) Negative covariation between task-related responses in alpha/beta-band activity and BOLD in human sensorimotor cortex: an EEG and fMRI study of motor imagery and movements. *Neuroimage* 49:2596–2606. doi: [10.1016/j.neuroimage.2009.10.028](https://doi.org/10.1016/j.neuroimage.2009.10.028)